Current-induced magnetization switching in a magnetic topological insulator heterostructure

Erik Zimmermann,* Justus Teller,* Michael Schleenvoigt, Gerrit Behner, Peter Schüffelgen, Hans Lüth, Detlev Grützmacher, and Thomas Schäpers†

Peter Grünberg Institut (PGI-9), Forschungszentrum Jülich, 52425 Jülich, Germany
and JARA-Fundamentals of Future Information Technology, Jülich-Aachen Research Alliance, Forschungszentrum Jülich and RWTH Aachen University, 52425 Jülich, Germany

(Received 18 August 2023; accepted 18 January 2024; published 20 February 2024)

We present the current-induced switching of the internal magnetization direction in a magnetic topological insulator/topological insulator heterostructure in the quantum anomalous Hall regime. The switching process is based on the bias current dependence of the coercive field, which is attributed to either Joule heating or the effect of the spin transfer provided by the unpolarized bias current. Increasing the bias current leads to a decrease in the magnetic order in the sample. When the applied current is subsequently reduced, the magnetic moments align with an externally applied magnetic field, resulting in repolarization in the opposite direction. This includes a reversal of the spin polarization and hence a reversal of the chiral edge mode. Possible applications in spintronic devices are discussed.

DOI: 10.1103/PhysRevMaterials.8.026201

I. INTRODUCTION

The quantum anomalous Hall effect (QAHE) is characterized by a vanishing longitudinal resistivity and a quantization of the Hall resistance at $h/e^2 \approx 25.8\ \mathrm{k\Omega}$ [1]. In this regime a single chiral edge channel and a bulk-insulating behavior are created by the interplay of electrons and an internal magnetization pointing perpendicular to the sample plane [2]. This effect was first observed in 2013 by Chang *et al.* [3] in thin films of ferromagnetic Cr-doped topological insulator material $(\mathrm{Bi,Sb})_2\mathrm{Te}_3$. Since then, the QAHE has been observed at low temperatures in several Cr- and V-based magnetic topological insulators (MTIs) [1,4–8]. The related chiral edge mode could possibly be a suitable basis for Majorana-based applications when combined with a superconductor, which makes MTIs promising candidates for future topological quantum computation operations [9–14].

The relevance of the applied current in MTI-based structures is underlined by recent reports about the breakdown of the QAHE dependent on the applied current and the dimensions of the sample. The latter gains importance, especially when aiming for nanostructures [6,15]. In this paper we investigate the current dependence of MTI magnetotransport properties. Current sweeps at fixed magnetic fields are used to switch the branch in the hysteresis only by changing the bias current. The experiment is completed by measurements at several different magnetic fields which allow a detailed investigation of the switching properties. The underlying mechanism of the current-induced magnetization switching is attributed to the current dependence of the coercive magnetic field $\mu_0 H_c$.

II. EXPERIMENT

$\mathrm{Cr}_{0.21}\mathrm{Bi}_{0.51}\mathrm{Sb}_{1.28}\mathrm{Te}_3$ is used as the magnetic topological insulator material. In order to reduce the possible contributions from a bulk channel caused by additional disorder arising from the chromium, a trilayer heterostructure is formed [7]. As shown in the sketch of the Hall bar structure in Fig. 1(a), a nonmagnetic topological insulator (TI) layer is sandwiched in between a top and bottom MTI layer to form an MTI/TI heterostructure. Here, a ternary compound with a stoichiometry of $\mathrm{Bi}_{0.55}\mathrm{Sb}_{1.45}\mathrm{Te}_3$ is chosen for the nonmagnetic TI interlayer.

For the growth of the MTI/TI heterostructure, a Si(111) substrate is cleaned using a piranha solution, followed by 1% hydrofluoric acid in order to remove native oxides and passivate the surface. Subsequently, the sample is loaded into a molecular beam epitaxy (MBE) chamber and heated to 700 °C to desorb the hydrogen passivation. After cooling the substrate down to the growth temperature of 220 °C within 30 min, first a Te flux is supplied for 30 s to repassivate the surface and prepare the sample for the subsequent layer growth. Next, Cr is provided from a standard Knudsen cell, set to 1045 °C, while Bi and Sb fluxes are added in a ratio of about Bi:Sb:Te 1:3:42 resulting in a MTI growth rate of 0.33 nm/min. Rutherford backscattering spectrometry (RBS) measurements on MTI films grown with these parameters yield the aforementioned stoichiometry of $\mathrm{Cr}_{0.21}\mathrm{Bi}_{0.51}\mathrm{Sb}_{1.28}\mathrm{Te}_3$. Additionally, layers grown with the same parameters but without Cr flux yield a stoichiometry of $\mathrm{Bi}_{0.55}\mathrm{Sb}_{1.45}\mathrm{Te}_3$ via RBS. The trilayer heterostructure is created by supplying Bi and Sb for 1 min to initialize TI growth, adding Cr flux for 5 min, closing the Cr shutter for 12 min, and lastly reopening the shutter for another 5 min. The total thickness of the trilayer amounts to 7.3 nm, divided into 1.6 nm MTI/4 nm TI/1.6 nm MTI, nominally. As a last step, a layer of 5 nm $\mathrm{Al}_2\mathrm{O}_3$ is deposited *in situ* via

*These authors contributed equally to this work.
†th.schaepers@fz-juelich.de

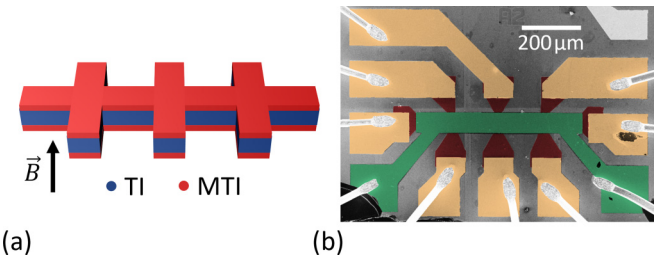

FIG. 1. MTI Hall bar sample. (a) A sketch of the Hall bar indicates the layering of MTI and conventional TI in the heterostructure. (b) A false-color scanning electron microscope image of the Hall bar depicts the MTI Hall bar (red), the top gate (green), and the metal contacts (orange). Note that the center part of the Hall bar is completely covered by the gate and has a width of 10 µm.

electron beam evaporation in order to prevent the sample from oxidation.

Subsequently, the MTI/TI heterorstructure is etched into a Hall bar shape using reactive ion etching and 50 nm Ti/100 nm Pt metal contacts are deposited via metal sputtering. The Hall bar structure has a width of 10 µm. The neighboring side contacts of the Hall bar are spaced by a distance of 150 µm. Using atomic layer deposition, 15 nm of HfO_2 are deposited globally as a dielectric layer. Lastly, a 50 nm Ti/100 nm Au gate is placed on top. The final device is depicted in Fig. 1(b).

The magnetotransport measurements are performed in a variable temperature insert cryostat with a base temperature of 1.3 K and a 14 T superconducting magnet. The magnetic field $\mu_0 H$ is oriented perpendicular to the substrate. All measurements are conducted using standard lock-in techniques in a four-terminal setup at the base temperature. A voltage of 2 V is applied to the top gate for all measurements since under these conditions the sample is in the regime of the QAHE (cf. Supplemental Material [16]; see Refs. [17–20] for the gate dependence of the QAHE).

III. RESULTS AND DISCUSSION

A. Current dependence

First, the current dependence of the magnetotransport properties of the Hall bar sample is presented. Figure 2(a) shows the transversal resistivity ρ_{xy} as a function of a perpendicular magnetic field for different applied currents ranging nonlinearly from 100 pA up to 1 µA. (See Supplemental Material [16] for the current dependence of ρ_{xx}.) All curves show a pronounced hysteresis. The coercive magnetic field $\mu_0 H_c$ substantially decreases with increasing current above 10 nA, indicating a weakening of the magnetism in the sample. The current dependence of $\mu_0 H_c$ is shown in Fig. 2(b). The transversal resistivity saturates at a value of 25 kΩ at a bias current of 0.1 nA close to the quantized value of h/e^2. Compared to the large decrease of the coercive field with bias currents above 10 nA, ρ_{xy} only decreases gradually reducing by 6% at 1 µA. (See Supplemental Material [16]). Similar results are presented by Kawamura *et al.* [8]. Since we found a saturation value ρ_{xy} close to h/e^2, transport can be assumed to take place in the QAHE regime with a high current

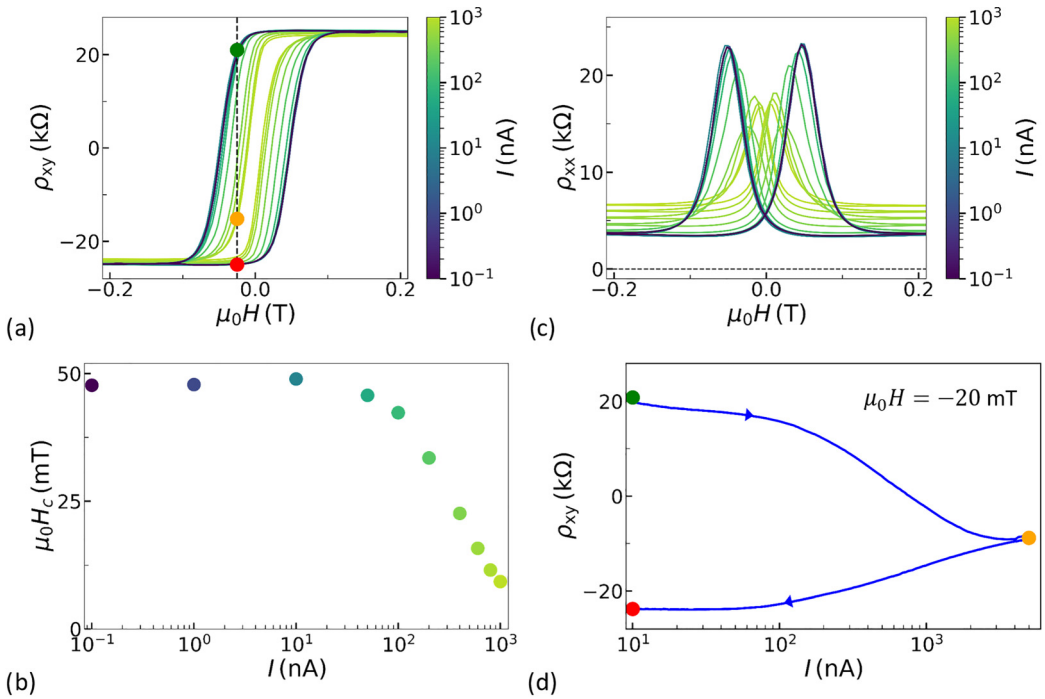

FIG. 2. Current dependence of the magnetotransport properties of the MTI/TI heterostructure. (a) Transversal resistivity ρ_{xy} as a function of magnetic field for different applied currents: 0.1, 1.0, 10, 50, 100, 200, 400, 600, 800, and 1000 nA. Note: The color code for the current is logarithmic. (b) The current dependence of the coercive magnetic field $\mu_0 H_c$ is plotted. (c) Corresponding longitudinal resistivity ρ_{xx} as a function of the magnetic field for the same current values as in (a). (d) For a constant magnetic field of −20 mT starting at the green dot the current is ramped up from 10 nA to 5 µA (yellow dot). Afterwards, the current is lowered again to the initial value of 10 nA (red dot).

density in the chiral edge channel. However, due to the finite longitudinal resistivity, a small current contribution can be assigned to bulk transport.

Figure 2(c) shows the longitudinal resistivity ρ_{xx} for different applied currents. The longitudinal resistivity also shows a hysteretic behavior with a peak at the magnetic field position where the magnetization reverses. As indicated by the colors in the plot, one can see that the shape of the hysteresis changes mostly for currents above 10 nA. With increasing bias current the peak that indicates the switching of the magnetization direction becomes less pronounced and the remaining resistivity at elevated magnetic fields is further increased. The finite resistance, as well as the increase in resistance with increasing applied current at elevated magnetic fields, can be explained by the presence of local charge puddles in between the edge channels on both sides of the Hall bar structure [21–23]. Here, the remaining thermal energy and the applied potential arising from the current and the finite resistance cause a growth of the puddles leading to a conducting connection across the sample and therefore create a finite resistance [6].

There are two possible origins of the dependence of the coercive magnetic field on the current: On the one hand, spin transfer caused by injecting an unpolarized current can lead to a randomization of the spin direction in the magnetic area for increased biases [24,25]. According to Berger [24], current entering the interface of a ferromagnet transfers its spin under an exchange force to align with the magnetic polarization. Misaligned electron transfer to localized magnetic moments and destabilize the magnetization. Indeed, an unpolarized current applied to a spin-polarized domain can even create a spin polarization in the opposite direction close to the magnetic domain due to spin-dependent reflection and transmission properties [26]. On the other hand, Joule heating arising from the previously mentioned enhanced current density could cause a decrease in the binding energy of the magnetic moments and thus a decrease of H_c. From our measurements we cannot conclusively determine if either spin-orbit torque or Joule heating is dominating. Probably it is a mixture of both. As shown in the Supplemental Material [16], for magnetic fields in the saturation region, i.e., 0.5 T, ρ_{xy} remains almost constant up to currents of 1 μA, whereas it drops rather rapidly with increasing temperature (see Supplemental Material [16]). Thus the current is apparently insufficient to cause a significant change in ρ_{xy}, even if the current leads to Joule heating. However, our switching process occurs at relatively small magnetic fields close to zero, where the magnetization is weaker and the chiral edge channels are probably less stable. Nevertheless, it can be assumed that the current bias causes only local heating because it is carried by the chiral edge channels, as opposed to global heating of the sample by raising the temperature.

B. Magnetization switching

In the previous section the impact of the applied current on the coercive field of our MTI/TI heterostructure was discussed. Up to this point, only magnetic field sweeps at different constant currents have been performed. Now, at constant magnetic fields the current is changed. It is expected that the bias current affects the magnetization in the transition region around $\mu_0 H = 0$ and thus the corresponding transversal resistivity ρ_{xy}. Three colored points at a constant magnetic field in Fig. 2(a) indicate hallmarks of the experiment. For initialization, the magnetic moments in the sample are first polarized by a positive magnetic field so that ρ_{xy} saturates. Subsequently, the magnetic field is ramped to a value of −20 mT so that at small bias currents ρ_{xy} settles at a value indicated by the green dot. As discussed in the previous section, an increased current lowers the coercive magnetic field. Following the dashed line in Fig. 2(a), ρ_{xy} decreases with increasing applied current. If the current is sufficiently large, the resistivity decreases from positive to negative values (yellow dot). This corresponds to a reversal of the majority of the magnetic moments in our MTI/TI heterostructure. When finally lowering the current to its initial value, more magnetic moments in the MTI get aligned to the externally applied magnetic field. The result is a complete reversal of magnetization (red dot).

An exemplary sequence of changing ρ_{xy} by driving the current back and forth between low and high values can be traced in Fig. 2(d). The sequence starts with a current of $I = 10$ nA at a constant magnetic field of $\mu_0 H = -20$ mT (green dot). Due to the curvature of the hysteresis the value of ρ_{xy} has already reduced slightly compared to its saturation value. As the current is increased, one finds that first the applied current slowly reduces the value of ρ_{xy}. When passing $\rho_{xy} = 0$ the current reduces the coercive magnetic field below the absolute value of the externally applied magnetic field. Upon increasing the current to 5 μA the magnetic moments predominantly switch their direction and align with the external magnetic field (yellow dot). When reducing the current again, the polarization is fully reversed (red dot). Thus, switching the direction of the magnetization is achieved by only varying the applied current. Hereby, the result for the transport is that the chiral edge mode is inverted.

In order to get a deeper insight into the switching mechanism, the sequence described in connection with Fig. 2(d) is run for different fixed magnetic fields $|\mu_0 H| \leqslant 60$ mT with a stepping of 5 mT. In Fig. 3(a) the initial and final values of ρ_{xy} (red and green dots, respectively) as well as the values at the maximum applied bias current (yellow dots) are plotted at the according magnetic field values, similarly to the ones in Fig. 2(a). As a reference the 10 nA hysteresis curve from Fig. 2(a) is also plotted in the same graph. The green dots representing the starting values lie quite well on the reference hysteresis curve, as expected, whereas the curve following the red dots for the final values is centered around zero magnetic field. Compared to that, the curve following the yellow dots corresponding to the maximum bias current of 5 μA comprises a smaller amplitude swing. One finds that for magnetic fields not too close to zero, i.e., larger than about 10 mT, and smaller than the coercive field, a switching occurs, since at elevated currents the sign of ρ_{xy} and by that the direction of the magnetization is inverted. Upon returning the bias current to 10 nA this magnetization orientation is kept. Hence, there is a successful switching of the branch obtained only by applying a pulse of a larger current.

In Fig. 3(b) the data for three representative curves are plotted against the applied current. Starting in the lower branch of the hysteresis, for curves at moderate magnetic fields at 20 mT, the same switching behavior as in Fig. 2(d) is found,

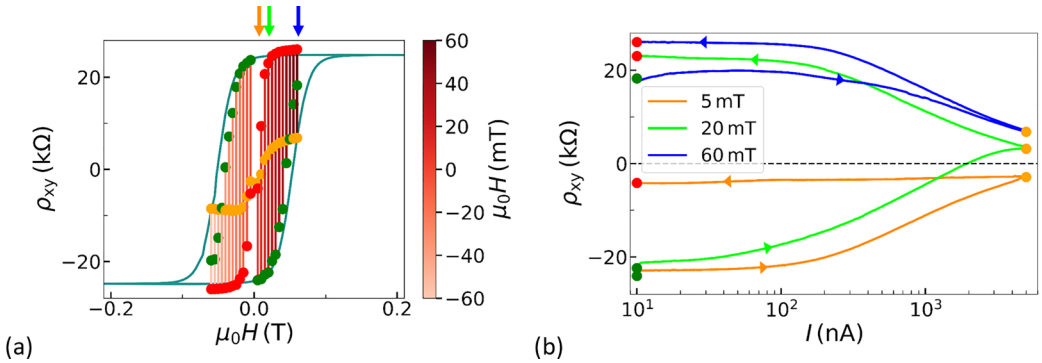

FIG. 3. Current-induced magnetization switching experiment for different magnetic bias fields. (a) The curves show ρ_{xy} for current sweeps from 10 nA (green dots) to 5 μA (yellow dots) back to 10 nA (red dots) at constant magnetic fields ranging from −60 to 60 mT in steps of 5 mT. The hysteresis of ρ_{xy} for a bias current of 10 nA, taken from Fig. 2(a), is plotted as a reference. (b) The current dependence of three representative curves from (a) at 5, 20, and 60 mT are compared.

i.e., the sign of ρ_{xy} and the direction of magnetization is inverted. In contrast, very close to zero magnetic field it is observed that the switching process fails, as indicated in Fig. 3(b) exemplarily by the curve recorded at $\mu_0 H = 5$ mT. Thus, at small magnetic fields the external magnetic field is insufficient to realign the magnetic moments in a ferromagnetic order. Also for fields larger than the coercive field, i.e., 60 mT in Fig. 3(b), where the magnetization is already aligned to the external field, the magnetization is weakened by the bias current but keeps its orientation. After returning to 10 nA even the saturation value of ρ_{xy} is reached, which is larger that the initial value.

It becomes apparent that the increased current weakens or even destroys the alignment of the magnetic moments, as indicated by the sequence of yellow dots in Fig. 3(a) being lower in amplitude than the initial hysteresis curve. We assume that at these large bias currents the carrier transport mainly takes place in the bulk [6]. When the current is lowered again the external magnetic field is responsible for the realignment in the opposite direction. For the curves at low and high magnetic fields one can see that no switching across zero occurs, but $|\rho_{xy}|$ first decreases below the starting value due to a reduction on magnetic order caused by the applied current for a given external magnetic field. Nonetheless, using this procedure also for the curves taken at larger magnetic fields, a switching of the other branch of the hysteresis occurs, thus stabilizing the magnetization to the saturation value. In this sense, the current bias can not only be employed to reverse the magnetization but in general be used to switch the magnetization to saturation with a significantly reduced external magnetic field.

IV. CONCLUSION

The current dependence of the coercive magnetic field of an MTI/TI heterostructure was employed in order to switch the direction of the internal magnetization by varying the bias current. It is concluded that after the reduction of the magnetic order with the use of an applied current the magnetic moments select the energetically favorable state which corresponds to an alignment along the external magnetic field. It is concluded that no magnetization is created in the process. Instead, only the direction is switched when comparing the start and end point. Around zero magnetic field, where the procedure fails, it can be seen that the effect is caused by an interplay of the current ramp and external magnetic field as here the external magnetic field is insufficient to repolarize the magnetic moments. For magnetic fields above the coercive fields no reversal of the magnetization takes place. However, in this case a stabilization into the other branch of the hysteresis is achieved.

In other current-induced magnetization switching experiments the magnetization direction can be switched back to the initial orientation by reversing the current. For the presented sample, however, the switching back to the initial magnetization needs a reversal of the externally applied magnetic field [27,28]. Thus, in principle, switching binary states is feasible. Since the externally applied magnetic field is small, it is possible to create small feature sizes. Additionally, a targeted application of current enables selectivity of specific memory cells. We want to point out that many important characteristics for spintronic applications (e.g., read/write speed, volatility, energy consumption, and information density) still need to be determined for this effect in future publications. Apart from the bias current-induced reversal of the magnetization in a certain magnetic field range, in general the current bias can also be employed to switch the magnetization to a stable state at significantly reduced external magnetic fields. It is indeed remarkable that without the assistance of the current sweep much larger magnetic fields are necessary to switch to the other branch of the ρ_{xy} hysteresis. This current-induced switching mechanism might be interesting for magnetic memory applications. In future experiments the switching effect observed here should be investigated with samples of different sizes and geometries in order to create tailored spintronic devices.

ACKNOWLEDGMENTS

We thank Herbert Kertz for technical assistance. All samples have been prepared at the Helmholtz Nano Facility [29]. This work is funded by the Deutsche Forschungsgemeinschaft (DFG, German Research Foundation) under Germany's Excellence Strategy – Cluster of Excellence Matter and Light for Quantum Computing (ML4Q) EXC 2004/1 – 390534769,

by the German Federal Ministry of Education and Research (BMBF) via the Quantum Futur project "MajoranaChips" (Grant No. 13N15264) within the funding program Photonic Research Germany and by the QuantERA grant MAGMA via the Deutsche Forschungsgemeinschaft under (Grant No. 491798118).

[1] C.-Z. Chang, C.-X. Liu, and A. H. MacDonald, Rev. Mod. Phys. **95**, 011002 (2023).
[2] S. Oh, Science **340**, 153 (2013).
[3] C.-Z. Chang, J. Zhang, X. Feng, J. Shen, Z. Zhang, M. Guo, K. Li, Y. Ou, P. Wei, L.-L. Wang, Z.-Q. Ji, Y. Feng, S. Ji, X. Chen, J. Jia, X. Dai, Z. Fang, S.-C. Zhang, K. He, Y. Wang, L. Lu *et al.*, Science **340**, 167 (2013).
[4] L. Zhang, D. Zhao, Y. Zang, Y. Yuan, G. Jiang, M. Liao, D. Zhang, K. He, X. Ma, and Q. Xue, APL Mater. **5**, 076106 (2017).
[5] C.-Z. Chang, W. Zhao, D. Y. Kim, H. Zhang, B. A. Assaf, D. Heiman, S.-C. Zhang, C. Liu, M. H. W. Chan, and J. S. Moodera, Nat. Mater. **14**, 473 (2015).
[6] G. Lippertz, A. Bliesener, A. Uday, L. M. C. Pereira, A. A. Taskin, and Y. Ando, Phys. Rev. B **106**, 045419 (2022).
[7] M. Mogi, R. Yoshimi, A. Tsukazaki, K. Yasuda, Y. Kozuka, K. S. Takahashi, M. Kawasaki, and Y. Tokura, Appl. Phys. Lett. **107**, 182401 (2015).
[8] M. Kawamura, M. Mogi, R. Yoshimi, A. Tsukazaki, Y. Kozuka, K. S. Takahashi, M. Kawasaki, and Y. Tokura, Phys. Rev. B **102**, 041301(R) (2020).
[9] I. Adagideli, F. Hassler, A. Grabsch, M. J. Pacholski, and C. W. J. Beenakker, SciPost Phys. **8**, 013 (2020).
[10] F. Hassler, A. Grabsch, M. J. Pacholski, D. O. Oriekhov, O. Ovdat, İ. Adagideli, and C. W. J. Beenakker, Phys. Rev. B **102**, 045431 (2020).
[11] T. Liu, J. J. He, and F. Nori, Phys. Rev. B **98**, 245413 (2018).
[12] C.-Z. Chen, Y.-M. Xie, J. Liu, P. A. Lee, and K. T. Law, Phys. Rev. B **97**, 104504 (2018).
[13] Y. Zeng, C. Lei, G. Chaudhary, and A. H. MacDonald, Phys. Rev. B **97**, 081102(R) (2018).
[14] C. W. J. Beenakker, P. Baireuther, Y. Herasymenko, I. Adagideli, L. Wang, and A. R. Akhmerov, Phys. Rev. Lett. **122**, 146803 (2019).
[15] E. J. Fox, I. T. Rosen, Y. Yang, G. R. Jones, R. E. Elmquist, X. Kou, L. Pan, K. L. Wang, and D. Goldhaber-Gordon, Phys. Rev. B **98**, 075145 (2018).
[16] See Supplemental Material at http://link.aps.org/supplemental/10.1103/PhysRevMaterials.8.026201 for the temperature dependence of the transport data, the properties of a single Cr-doped layer, the gate dependence of the longitudinal and transversal conductivities, and the current-induced switching of the longitudinal resistivity.
[17] M. Onoda and N. Nagaosa, Phys. Rev. Lett. **90**, 206601 (2003).
[18] C. Niu, N. Mao, X. Hu, B. Huang, and Y. Dai, Phys. Rev. B **99**, 235119 (2019).
[19] Y. Deng, Y. Yu, M. Z. Shi, Z. Guo, Z. Xu, J. Wang, X. H. Chen, and Y. Zhang, Science **367**, 895 (2020).
[20] S. Zhang, R. Wang, X. Wang, B. Wei, B. Chen, H. Wang, G. Shi, F. Wang, B. Jia, Y. Ouyang *et al.*, Nano Lett. **20**, 709 (2020).
[21] N. Ito, R. Masutomi, and T. Okamoto, Phys. Rev. B **105**, 205434 (2022).
[22] T. Knispel, W. Jolie, N. Borgwardt, J. Lux, Z. Wang, Y. Ando, A. Rosch, T. Michely, and M. Grüninger, Phys. Rev. B **96**, 195135 (2017).
[23] N. Borgwardt, J. Lux, I. Vergara, Z. Wang, A. A. Taskin, K. Segawa, P. H. M. van Loosdrecht, Y. Ando, A. Rosch, and M. Grüninger, Phys. Rev. B **93**, 245149 (2016).
[24] L. Berger, J. Appl. Phys. **55**, 1954 (1984).
[25] C. H. Marrows, Adv. Phys. **54**, 585 (2005).
[26] V. K. Dugaev, J. Berakdar, and J. Barnaś, Phys. Rev. B **68**, 104434 (2003).
[27] K. Cai, M. Yang, H. Ju, S. Wang, Y. Ji, B. Li, K. W. Edmonds, Y. Sheng, B. Zhang, N. Zhang, S. Lui, H. Zheng, and K. Wang, Nat. Mater. **16**, 712 (2017).
[28] L. Liu, Q. Qin, W. Lin, C. Li, Q. Xie, S. He, X. Shu, C. Zhou, Z. Lim, J. Yu, W. Lu, M. Li, X. Yan, S. J. Pennycook, and J. Chen, Nat. Nanotechnol. **14**, 939 (2019).
[29] W. Albrecht, J. Moers, and B. Hermanns, J. large-scale Res. Fac. JLSRF **3**, A112 (2017).